Available online at www.sciencedirect.com
SCIENCE DIRECT
Journal of Catalysis 234 (2005) 206–218
JOURNAL OF CATALYSIS
www.elsevier.com/locate/jcat

Sulfur deactivation of Pt/SiO_2, $Pt/BaO/Al_2O_3$, and BaO/Al_2O_3 NO_x storage catalysts: Influence of SO_2 exposure conditions

Jazaer Dawody [a,b,*], Magnus Skoglundh [a,c], Louise Olsson [a,c], Erik Fridell [a,b]

[a] *Competence Centre for Catalysis, Chalmers University of Technology, SE-412 96 Göteborg, Sweden*
[b] *Department of Applied Physics, Chalmers University of Technology, SE-412 96 Göteborg, Sweden*
[c] *Department of Chemical and Biological Engineering, Chalmers University of Technology, SE-412 96 Göteborg, Sweden*

Received 19 February 2005; revised 18 May 2005; accepted 29 May 2005

Available online 21 July 2005

Abstract

Flow reactor experiments were performed to study the effect of $SO_2 + O_2$ and $SO_2 + H_2$ exposures on the NO_x storage performance of $Pt/BaO/Al_2O_3$ and BaO/Al_2O_3 catalysts. In addition, Pt/SiO_2 samples were used to study the interaction between Pt and SO_2 under the two exposure conditions. For BaO/Al_2O_3 the two SO_2 exposure conditions caused similar deactivation of the NO_x storage capacity, whereas for $Pt/BaO/Al_2O_3$ the decline in the NO_x storage capacity was faster during the $SO_2 + H_2$ exposure than for $SO_2 + O_2$ exposure. The presence of Pt enhances the adsorption of SO_2 for both SO_2 exposure conditions. Quantitative analysis of sulfur showed that exposure to $SO_2 + O_2$ caused higher accumulation of sulfur in $Pt/BaO/Al_2O_3$ samples in comparison with $SO_2 + H_2$ exposure. Thus there is no correlation between the total amount of adsorbed sulfur in the samples and the reduction of the NO_x storage capacity, probably because of the adsorption of sulfur on sites not necessarily important for the NO_x storage process.

Keywords: NO_x storage catalysts; Sulfur deactivation; Pt; BaO; Al_2O_3; SiO_2; SO_2

1. Introduction

Lean-burn gasoline and diesel engines offer good fuel economy and relatively low CO_2 emissions [1]. However, the presence of large amounts of oxygen in lean-burn and diesel exhausts prevents effective reduction of nitrogen oxides (NO_x) to nitrogen, since the reducing agents in the exhausts are more favorably oxidized by oxygen than by NO_x [2]. To solve this problem, new abatement technologies have been developed, one of which is NO_x storage technology.

The NO_x storage concept is based on incorporation of a storage component into the three-way catalyst (TWC) to store NO_x during lean conditions for a time period of minutes. To regenerate the storage sites, the conditions are switched to rich (oxygen deficit) for a few seconds. The stored NO_x is then released and subsequently reduced over precious metal sites to N_2 by the reducing agents (CO, HC, H_2) [3]. A typical NO_x storage catalyst consists mainly of precious metals such as Pt, Pd, and Rh; a NO_x storage component, usually BaO; and a high-surface-area support like Al_2O_3 on which the precious metal(s) and the storage component(s) are dispersed.

The research regarding the NO_x storage systems comprises investigations of the processes during the storage and regeneration phases and provides good understanding of the catalytic performance of such systems [3–20]. However, great efforts are still needed to improve the performance of the NO_x storage catalysts because of their sensitivity toward sulfur. The presence of sulfur in the fuel and lubricants, even in low concentrations, poisons the catalysts by the formation of stable sulfates with the NO_x storage compounds [21–25]. The decomposition and elimination of sulfate require high temperature treatment [26], which in turn may cause the stor-

* Corresponding author. Fax: +46-31-7723134.
E-mail address: jazaer.dawody@fy.chalmers.se (J. Dawody).

0021-9517/$ – see front matter
doi:10.1016/j.jcat.2005.05.017

age material to deteriorate and decrease the storage capacity [27]. Sulfur also influences the catalytic activity over the noble metal sites [23,28] and can increase the sintering [29]. Studies of sulfur deactivation of NO_x storage catalysts have shown that (i) the deactivation increases with increased sulfur exposure time or dose [24]; (ii) compounds such as H_2S and COS deactivate the NO_x storage capacity in a way that is similar to the way in which SO_2 does [30,31]; (iii) between 250 and 450 °C the exposure to SO_2 decreases the catalytic activity for NO oxidation and the reduction capacity of the precious metal during rich conditions through the accumulation of sulfur-containing species on the precious metal sites [23]; (iv) the rate of sulfur deactivation is higher under rich conditions than during lean exposure [32]; (v) exposure to SO_2 or $SO_2 + O_2$ results in the formation of $BaSO_4$ by a gradual removal of $BaCO_3$ [30,33]; (vi) small $BaSO_4$ particles are more easily decomposed than large $BaSO_4$ particles [34]; and (vii) the decomposition of $BaSO_4$ requires high-temperature treatment [35], but the presence of water decreases the decomposition temperature of $BaSO_4$ [26].

It has been suggested that the sulfate formation proceeds via the oxidation of SO_2 to SO_3, which reacts with the BaO and Al_2O_3 to form barium and aluminum sulfate, respectively [25]. In a previous work, we found that addition of MoO_3 to Pt/Al_2O_3 enhances the oxidation of NO while suppressing the SO_2 oxidation. However, when MoO_3 was added to a $Pt/BaO/Al_2O_3$ catalyst, the sulfur deactivation for the modified catalyst proceeded faster than for the unmodified $Pt/BaO/Al_2O_3$ catalyst [5]. From this and (iv) above it is clear that there is no simple correlation between SO_3 formation and deactivation of the NO_x storage capacity.

In this work we have investigated the influence of the SO_2 exposure conditions on the deactivation of the NO_x storage performance. The SO_2 exposure conditions were chosen to be SO_2 only, $SO_2 + O_2$, and $SO_2 + H_2$. Sulfur deactivation may take place by the accumulation of sulfur-containing species on three sites that are important for NO_x storage: (1) Pt sites, (2) surface storage sites, and (3) bulk storage sites. Pt/SiO_2 samples were used to study the interaction between SO_2 and Pt under the different exposure conditions, since silica has a low affinity for sulfur. For SO_2 interaction with the two kinds of NO_x storage sites, $Pt/BaO/Al_2O_3$ and BaO/Al_2O_3 samples were used. The experiments and gas feeds used in this work are designed for use in the construction of a micro-kinetic model for sulfur deactivation of NO_x storage catalysts. The model construction is greatly simplified if the number of catalyst components, as well as gas feed components, is reduced. However, the model will be extended gradually to include components important for the NO_x storage and sulfur deactivation. In this work we have chosen to exclude CO_2 and water vapor from the gas system in order to study the effect of SO_2 exposure under reducing and oxidizing conditions in the absence of these two gas compounds. Both CO_2 and H_2O significantly influence the NO_x storage performance [6]. Sulfur deactivation of NO_x storage catalysts has been observed both with [25,34,36–38] and without [23,28,30–33,39] H_2O. It has been found that sulfates are more easily reduced when H_2O is present in the gas mixture under rich conditions [26]. We plan to include CO_2 and water vapor in the gas feed in a forthcoming study and to use the results to extend the kinetic model to include the effect of these two gas compounds on the sulfur deactivation process.

2. Experimental

2.1. Sample preparation

Cordierite monoliths (400 cells per square inch) with a length of 20 mm, containing 188 channels, were used to prepare the catalysts used in this work. The preparation of the different types of catalysts is briefly described below. For more details on the preparation method, see Ref. [40].

2.1.1. $Pt/BaO/Al_2O_3$ and BaO/Al_2O_3 samples

We coated six monoliths with alumina by immersing them in an alumina slurry, blowing away excess slurry from the channels, drying them in air at 95 °C for few seconds, and calcining them in air at 500 °C for 2 min. This procedure was repeated until the desired amount of alumina was obtained. Thereafter, the samples were calcined at 600 °C for 2 h. The alumina-coated samples were then provided with barium by impregnation with aqueous $Ba(NO_3)_2$ solution, drying, and calcination. To avoid dissolution of BaO during the impregnation with the Pt solution, BaO was converted to $BaCO_3$, which is considerably less soluble in aqueous solutions than BaO. We transformed BaO to $BaCO_3$ by exposing the BaO/Al_2O_3 samples to air in closed sample holders. After 1 week the samples were immersed in a solution of ammonium carbamate for 1 h, dried in air at 130 °C, and calcined in air at 500 °C for 3 min. Three of the $BaCO_3/Al_2O_3$ samples were calcined for 2 h (starting at 200 °C and heating to 450 °C with 5 °C/min). The remaining three $BaCO_3/Al_2O_3$ samples were washed in distilled water and provided with a solution of Pt nitrate [$Pt(NO_3)_2$]. We performed the Pt impregnation by filling the channels with the desired amount of Pt, diluted in distilled water. The samples were then dried in air at 80 °C for 12 h and finally calcined for 2 h, starting at 200 °C, and heated to 450 °C at 5 °C/min. It is likely that $BaCO_3$ is transformed to BaO during the calcination or as an initial step before the NO_x storage. For this purpose, the samples with and without Pt are referred to as $Pt/BaO/Al_2O_3$ and BaO/Al_2O_3, respectively.

2.1.2. Pt/SiO_2 and SiO_2 samples

Five monoliths were coated with a silica sol (Bindzil 40NH_3 170) by the procedure used for the alumina coating and calcined at 500 °C for 2 h. Four of the samples were impregnated with a Pt solution of tetraammineplatinum

Table 1
Sample washcoat compositions, BET surface area and Pt dispersion

Sample	Al_2O_3 (mg)	SiO_2 (mg)	BaO (mg)	Pt (mg)	BET ($m^2/g_{washcoat}$)	Pt dispersion (%)
Pt/Si-1		1449		16.8	123	12.0
Pt/Si-2		930		16.8	122	11.3
Pt/Si-3		1051		16.8	120	11.9
Pt/Si-4		980		16.8	120	12.0
SiO_2		1020				
Pt/Ba/Al-1	597		140	16.9	113	20.4
Pt/Ba/Al-2	623		132	17.3	119	22.1
Pt/Ba/Al-3	606		131	17.9	121	21.1
Ba/Al-1	853		137		n.d.[a]	
Ba/Al-2	711		108		n.d.[a]	
Ba/Al-3	711		127		n.d.[a]	

[a] n.d. = not determined.

hydroxide [$Pt(NH_3)_4(OH)_2$]. The Pt impregnation and calcination were performed with the same procedure as for the $Pt/BaO/Al_2O_3$ samples.

The compositions of all samples used in this work are given in Table 1.

2.2. Catalyst characterization

The Pt dispersion of the $Pt/BaO/Al_2O_3$ and Pt/SiO_2 catalysts was determined with the use of N_2O dissociation. For each dissociated N_2O molecule, it is assumed that one gaseous N_2 molecule is formed and one oxygen atom is left on each surface Pt atom according to the following reaction [41]:

$$Pt_s + N_2O(g) \rightarrow Pt\text{–}O + N_2(g), \quad (1)$$

where Pt_s denotes a surface Pt atom. The experiments were conducted in a flow reactor with a quartz tube in which the catalyst was placed. A thermocouple used to control the temperature was placed 10 mm in front of the catalyst. Another thermocouple was placed inside the catalyst to measure the catalyst temperature. A mass spectrometer (Balzer QME 120) was connected to the reactor to analyze the outflow gas composition. The gas flow into the reactor was controlled with mass flow controllers. More details about this reactor can be found in Ref. [42].

Before each measurement, the catalyst was pre-oxidized for 10 min in 2% O_2 in Ar, flushed with Ar for 5 min, pre-reduced in 4% H_2 in Ar, and flushed with Ar for 10 min at 500 °C. The temperature was then decreased to 90 °C, and the catalyst was instantly exposed to 500 ppm N_2O in Ar (gas flow = 200 ml/min) for 20 min. We determined the Pt dispersion by integrating the N_2 ($m/e = 28$) signal during the N_2O exposure step after subtracting the m/e contribution that originates from the cracking of N_2O in the mass spectrometer.

The specific surface area of the catalysts was determined by nitrogen adsorption with the BET method, with the use of a Digisorb 2600 (Micromertics) instrument.

The Pt dispersion and the specific surface area of the catalysts are given in Table 1.

2.3. Activity measurements

All activity measurements were performed in a flow reactor with a quartz tube supplied with a heating coil connected to a power unit. The temperature was controlled with a PID regulator from Eurotherm and two thermocouples of type K from Pentronic. One thermocouple was placed 10 mm in front of the catalyst, and the other was placed inside the catalyst. The gas mixtures were prepared via an Environics 2000 gas blender containing nine separate mass flow controllers. The outlet flow was analyzed with a chemiluminescense detector (CLD 700) for NO and NO_2 and three nondispersive IR Maihak UNOR 610 instruments for SO_2, CO_2, and N_2O, respectively. A Labview program, specially designed for this equipment, was used to overview the temperature and gases via a PC. The gas flow and space velocity in all experiments were 3500 ml/min and 33 000 h^{-1}, respectively, with Ar as the carrier gas.

Before all activity measurements the samples were pretreated at 500 °C in 8% O_2 in Ar for 10 min, flushed with Ar for 5 min, and finally reduced in 1.8% H_2 in Ar for 20 min.

2.3.1. NO oxidation

The catalytic activity of the fresh Pt/SiO_2 and $Pt/BaO/Al_2O_3$ samples for NO oxidation was tested with temperature-programmed NO oxidation experiments. The pretreated catalysts were stabilized at room temperature in a reaction gas mixture consisting of 450 ppm NO and 8% O_2 in Ar for 1 h. Thereafter, the temperature of the reaction gas mixture increased linearly with 5 °C/min to 450 °C.

2.3.2. SO_2 oxidation

One of the Pt/SiO_2 samples (Pt/Si-1) was used for SO_2 oxidation. The pretreated catalyst was exposed to a reaction gas mixture consisting of 40 ppm SO_2 and 8% O_2 in Ar at 25 °C for 20 min. Thereafter the temperature of the reaction gas mixture was increased, and the activity for SO_2 oxidation was measured at steps from 50 to 600 °C with 50 °C between the steps and for 20 min at each step.

2.3.3. SO_2 exposure to SiO_2

The pretreated SiO_2 sample was exposed to sulfur at 300 °C for 10 min. The gas mixture during the three exposure conditions consisted of (1) 40 ppm SO_2 and 8% O_2 in Ar; (2) 40 ppm SO_2 in Ar; (3) 40 ppm SO_2 and 1.8% H_2 in Ar. After each exposure condition, the sample was flushed with Ar until no outlet SO_2 could be detected.

2.3.4. SO_2 exposure to Pt/SiO_2

Three of the Pt/SiO_2 samples were used to study the interaction between Pt and SO_2 under three different conditions. We did this by exposing each catalyst to SO_2, $SO_2 + O_2$, or $SO_2 + H_2$, flushing with Ar, increasing the temperature to 750 °C by 20 °C/min, and treating with oxygen for a few minutes. The Pt/Si-4 sample was exposed to 40 ppm SO_2 in

Ar, and Pt/Si-3 and Pt/Si-2 were exposed to 40 ppm SO_2 in combination with 8% O_2 or 1.8% H_2, respectively.

2.3.5. NO_x storage and regeneration

The NO_x storage capacity for all $Pt/BaO/Al_2O_3$ and BaO/Al_2O_3 samples was measured before the samples were exposed to sulfur. Three identical NO_x storage and regeneration cycles were performed for each sample. The storage cycles were performed at 300 °C with a gas mixture of 630 ppm NO_2 and 8% O_2 in Ar for 30 min per storage period. To regenerate the storage sites after each NO_x storage step, the samples were flushed with Ar for 10 min, and the temperature was linearly increased in Ar by 20 °C/min to 600 °C (750 °C in the case of BaO/Al_2O_3 samples).

2.3.6. SO_x and NO_x storage

The $Pt/BaO/Al_2O_3$ and BaO/Al_2O_3 samples were treated with sulfur under the same SO_2 exposure conditions as for the Pt/SiO_2 samples. For each SO_2 exposure condition, one $Pt/BaO/Al_2O_3$ and one BaO/Al_2O_3 sample were used. In the experiments the samples were exposed to sulfur at 300 °C for 20 min and flushed with Ar for 10 min, and a NO_x storage and regeneration cycle was performed as mentioned in Section 2.3.3. For the BaO/Al_2O_3 samples, the thermal regeneration was extended to 750 °C. Three sulfur and NO_x storage cycles were performed for each sample.

The amounts of sulfur accumulated in the samples that were treated with $SO_2 + O_2$ and $SO_2 + H_2$ were measured with a LECO SC-432 sulfur analyzer. The quantitative estimation of sulfur is based on high-temperature combustion (1370 °C), where all sulfur-containing compounds are oxidized to SO_2 and SO_3. SO_3 is subsequently reduced to SO_2, and the total amount of SO_2 is analyzed in an IR cell.

3. Results

3.1. NO oxidation over Pt/SiO_2 and $Pt/BaO/Al_2O_3$

The measured NO, NO_2, and NO_x outlet signals from temperature-programmed NO oxidation experiments for all four Pt/SiO_2, and three $Pt/BaO/Al_2O_3$ catalysts are displayed in Figs. 1a and 1b, respectively. The corresponding thermodynamic equilibrium NO and NO_2 concentrations are also shown in the figures. The measured NO and NO_2 concentrations follow the thermodynamic equilibrium at temperatures above 350 °C. For all four Pt/SiO_2 samples, the oxidation of NO starts at about 100 °C and reaches 50% conversion at about 160 °C. For the $Pt/BaO/Al_2O_3$ samples, the NO oxidation starts at about 100 °C and reaches 50% conversion at about 170 °C.

A comparison of the results in Figs. 1a and 1b shows an obvious difference in the NO_x responses for the two catalyst types. For the Pt/SiO_2 samples, the NO_x signal is constant during the entire experiment, whereas for the $Pt/BaO/Al_2O_3$ samples, the NO_x signal exceeds the inlet NO concentration

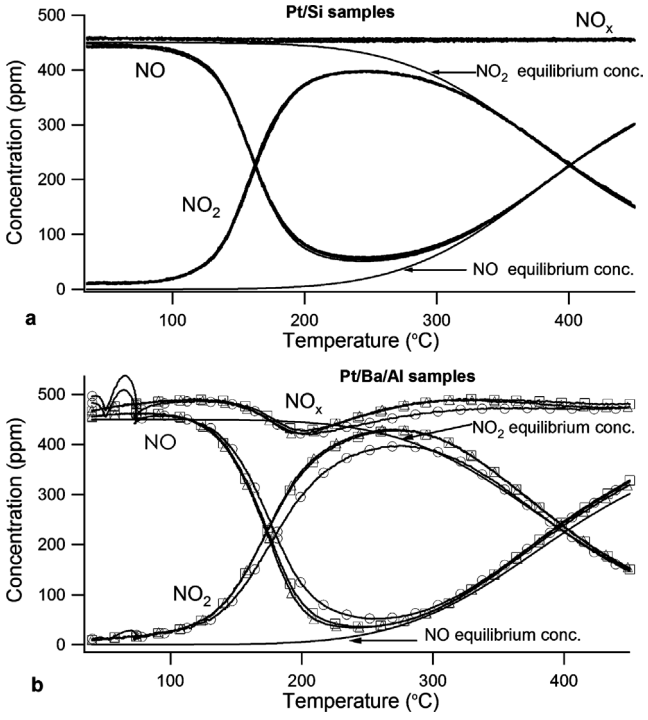

Fig. 1. NO, NO_2 and NO_x concentrations as a function of temperature during NO oxidation experiments performed on (a) four Pt/SiO_2 samples and (b) three $Pt/BaO/Al_2O_3$ samples (Pt/Ba/Al-1 (○), Pt/Ba/Al-2 (□), Pt/Ba/Al-3 (Δ)) with 450 ppm NO, 8% O_2 in Ar with a space velocity of 33 000 h^{-1}. Thermodynamic NO and NO_2 concentrations are given for comparison.

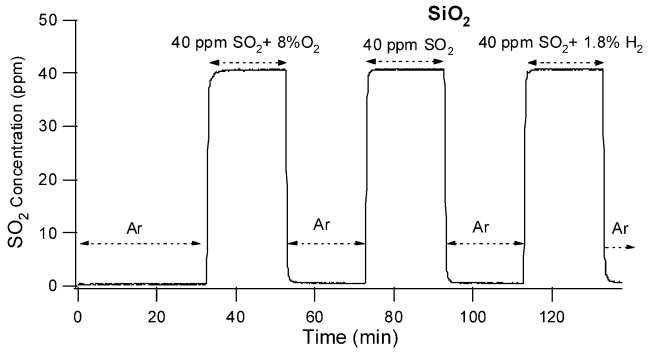

Fig. 2. SO_2 concentration as a function of time from exposing a SiO_2 sample to three SO_2 steps with 20 min/step. SO_2 steps: (1) 40 ppm SO_2 + 8% O_2; (2) 40 ppm SO_2; (3) 40 ppm SO_2 + 1.8% H_2.

as soon as the temperature ramp is started. As the temperature is further increased, the NO_x signal decreases to a minimum value and then increases again to a value slightly higher than the inlet NO concentration during the remaining time of the experiment.

3.2. Sulfur interaction with SiO_2 and Pt/SiO_2

Fig. 2 shows the results obtained for the SiO_2 sample and the three different sulfur exposures. Interestingly, the SO_2 outlet signal in all cases rapidly reaches the inlet level (40 ppm) as the SO_2 exposure starts.

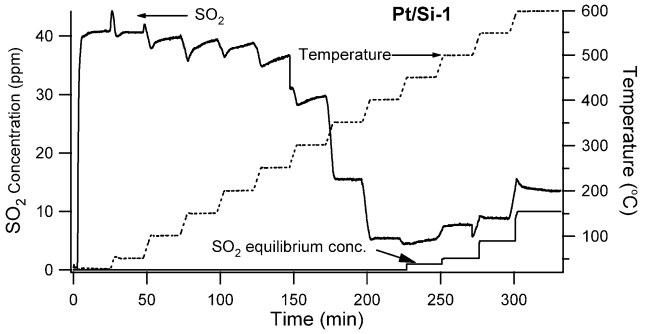

Fig. 3. SO_2 concentration and catalyst temperature as a function of time from temperature step SO_2 oxidation experiment performed by exposing a Pt/SiO_2 catalyst to 40 ppm SO_2 and 8% O_2 in Ar with a space velocity of 33,000 h^{-1}.

Fig. 3 shows the outlet SO_2 concentration and catalyst temperature as a function of time during a SO_2 oxidation experiment performed with one of the Pt/SiO_2 samples (Pt/Si-1). The thermodynamic equilibrium SO_2 concentration is also shown. It is worth mentioning that the obtained SO_2 concentration (measured by nondispersive IR spectroscopy) may be slightly higher than the true values because of the interference of IR peaks, since the characteristic SO_3 peak (at 1391 cm^{-1}) coincides with the measured SO_2 peaks. However, the experiment was performed to estimate the catalytic activity for SO_2 oxidation; thus approximate SO_2 concentrations are sufficient. From Fig. 3 it is clear that the SO_2 oxidation starts at about 200 °C and increases with increasing temperature up to 450 °C. At higher temperatures, the SO_2 concentration increases again with increasing temperature.

The results from $SO_2 + H_2$ and $SO_2 + O_2$ exposure experiments are shown in Figs. 4a and 4b, respectively. The result from the SO_2 exposure experiment is similar to that from the $SO_2 + O_2$ experiment. The change in the SO_2 signal during the $SO_2 + H_2$ exposure step is small and occurs mainly in the beginning of the step as a drop in the SO_2 signal from 12 to 9 ppm. However, the signal rises again, reaches 12 ppm, and remains almost constant until the end of the step. The amount of adsorbed and converted SO_2 during the $SO_2 + H_2$ step is ∼9 μmol; however, only 0.4 μmol SO_2 desorbs from the catalyst after the sulfur exposure step. A significant amount of SO_2 is detected during the O_2 treatment performed after the temperature ramp (see the SO_2 desorption peak at about 175 min). The SO_2 desorbing during the temperature ramp and the oxygen treatment corresponds to about 4% of the number of surface Pt sites.

The results from the $SO_2 + O_2$ exposure experiment (shown in Fig. 4b) show an increase in the outlet SO_2 with time. The SO_2 signal reaches 20 ppm (50% of the inlet concentration) after 14 min. Thereafter, the signal increases more slowly and reaches 29 ppm toward the end of the sulfur step. A well-resolved SO_2 desorption peak is seen at about 640 °C. Furthermore, no SO_2 is detected during the oxygen treatment step. The amount of converted and adsorbed sulfur during the entire experiment is ∼4.5 μmol, whereas 0.7 μmol

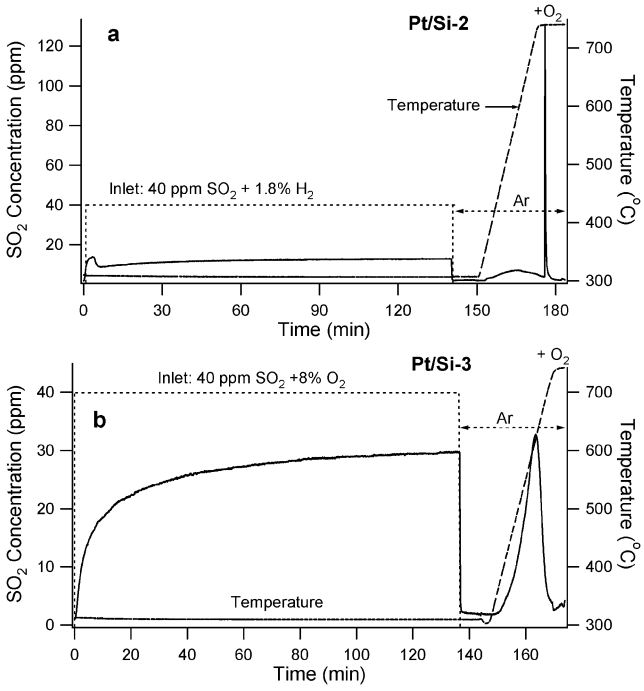

Fig. 4. SO_2 concentration and catalyst temperature as a function of time from SO_2 steps followed by temperature programmed desorption and O_2 treatment using one Pt/SiO_2 sample for each SO_2 exposure condition: (a) 40 ppm $SO_2 + 1.8\%$ H_2; (b) 40 ppm $SO_2 + 8\%$ O_2.

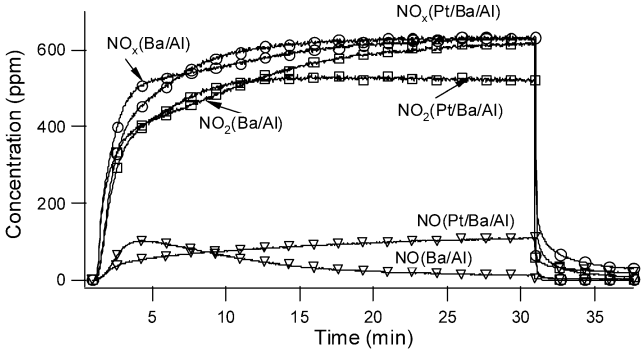

Fig. 5. NO, NO_2 and NO_x concentrations as a function of time from one $Pt/BaO/Al_2O_3$ sample and one BaO/Al_2O_3 sample during NO_x storage experiments using 630 ppm NO_2 and 8% O_2.

SO_2 is detected during the TPD, which corresponds to 6.7% of the surface Pt sites. No SO_2 desorption is detected during the treatment with O_2.

The quantitative sulfur analysis showed that no sulfur remained in Pt/Si-2 and Pt/Si-3 samples that were exposed to $SO_2 + H_2$ and $SO_2 + O_2$, respectively.

3.3. NO_x storage in $Pt/BaO/Al_2O_3$ and BaO/Al_2O_3 before exposure to sulfur

The outlet NO, NO_2, and NO_x signals obtained from Pt/Ba/Al-1 and Ba/Al-1, respectively, during a sulfur-free NO_x storage period are shown in Fig. 5. The NO_2 responses from the two samples are rather similar during the

first 12 min. Thereafter, the NO_2 signal from Ba/Al-1 increases with time, whereas the corresponding signal from the Pt/Ba/Al-1 remains stable. During the first minutes of the storage period, more NO is released from Ba/Al-1 compared with Pt/Ba/Al-1. However, with time the NO response from Ba/Al-1 declines to about 10 ppm, whereas the NO concentration after the Pt/Ba/Al-1 sample increases to ∼110 ppm. After about 17 min of the storage phase, the NO_x signal from Pt/Ba/Al-1 reaches the inlet NO_2 concentration, whereas for Ba/Al-1 the corresponding signal remains below the inlet concentration until the end of the storage phase.

3.4. Sulfur storage in $Pt/BaO/Al_2O_3$ and BaO/Al_2O_3

As mentioned in Section 2, the NO_x storage capacity for the $Pt/BaO/Al_2O_3$ and BaO/Al_2O_3 samples was first determined in a sulfur-free atmosphere. The samples were then exposed to sulfur before each NO_x storage cycle. Three such SO_x and NO_x storage cycles were performed for each sample. In Fig. 6 the outlet SO_2 concentration during the three cycles is presented as a function of time for $SO_2 + H_2$ and $SO_2 + O_2$ exposures. The results for the $Pt/BaO/Al_2O_3$ samples are shown in Figs. 6a and 6c, and the corresponding results for the BaO/Al_2O_3 samples are shown in Figs. 6b and 6d. The upper parts of the figures show the results from the $SO_2 + H_2$ exposure, and the lower parts show the results for the $SO_2 + O_2$ treatment. Obviously, the amounts of SO_2 detected under the two sets of SO_2 exposure conditions are much lower for the $Pt/BaO/Al_2O_3$ samples than for the BaO/Al_2O_3 samples. For $Pt/BaO/Al_2O_3$, no outlet SO_2 is detected upon exposure to SO_2 in combination with H_2, whereas during exposure to SO_2 in combination with O_2, minor amounts of SO_2 are detected in the third sulfur exposure step. In the absence of Pt (BaO/Al_2O_3 samples), there is still some SO_2 in the outlet gas even 10 min after the SO_2 supply has been turned off. Furthermore, the outlet SO_2 concentration during the $SO_2 + O_2$ exposure is significantly lower than during the $SO_2 + H_2$ exposure.

Fig. 7 shows the outlet SO_2 concentration as a function of temperature during the temperature ramps performed at the end of the storage cycles. Figs. 7a and 7c are for the $Pt/BaO/Al_2O_3$ samples, and Figs. 7b and 7d show the results for the BaO/Al_2O_3 samples. No SO_2 desorption is observed from Pt/Ba/Al-3, which was exposed to $SO_2 + H_2$, and a minor amount of SO_2 is detected during the third temperature ramp from Pt/Ba/Al-2, which was exposed to $SO_2 + O_2$. For the BaO/Al_2O_3 samples, no SO_2 desorption is observed after either SO_2 exposure condition.

The results from the quantitative sulfur analysis of $Pt/BaO/Al_2O_3$ and BaO/Al_2O_3 samples exposed to $SO_2 + O_2$ and $SO_2 + H_2$ are displayed in Table 3 (recall that the amounts of washcoat materials of the catalysts are given in

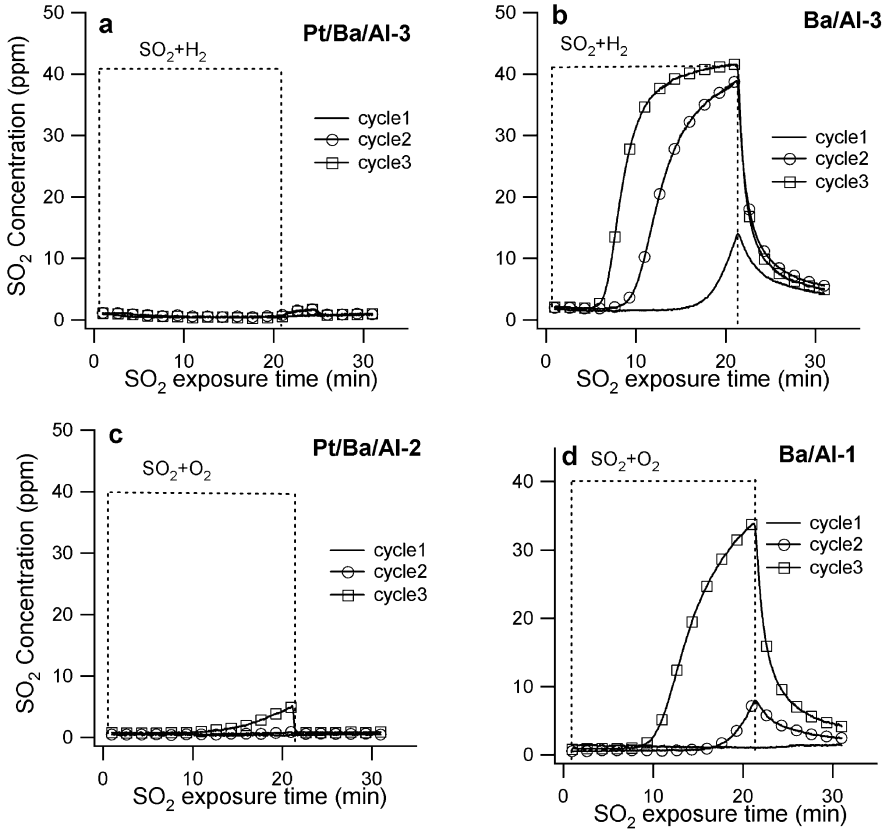

Fig. 6. SO_2 concentration as a function of time during three sulfur treatment cycles for each SO_2 exposure condition performed using $Pt/BaO/Al_2O_3$ and BaO/Al_2O_3 samples (one sample from each kind for each SO_2 exposure condition). SO_2 exposure conditions: (a) and (b): 40 ppm $SO_2 + 1.8\%$ H_2; (c) and (d): 40 ppm $SO_2 + 8\%$ O_2.

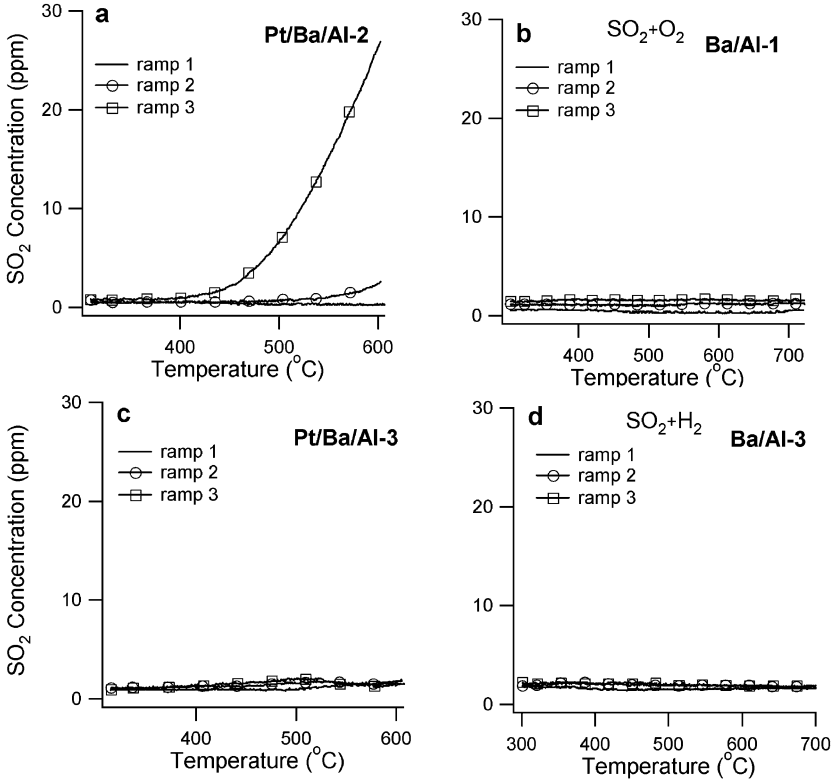

Fig. 7. SO_2 concentration as a function of temperature during three heating ramp treatments to desorb SO_2 after three SO_2 exposure cycles for each SO_2 exposure condition performed using $Pt/BaO/Al_2O_3$ and BaO/Al_2O_3 samples (one sample from each kind for each SO_2 exposure condition). SO_2 exposure conditions: (a) and (b): 40 ppm $SO_2 + 1.8\%$ H_2; (c) and (d): $SO_2 + 8\%$ O_2.

Table 2
Amount of stored NO_x for $Pt/BaCO_3/Al_2O_3$ and $BaCO_3/Al_2O_3$ samples. The SO_2 concentration was 40 ppm in all exposures. The H_2 and O_2 concentrations were 1.8 and 8%, respectively. NO_x storage cycles were conducted by exposing the catalysts to 630 ppm NO_2 and 8% O_2. Space velocity in all cases was 33 000 h^{-1}

Sample	SO_2 exposure condition	NO_x storage in relation to SO_2 exposure time (mmol/$g_{(BaO+alumina)}$)			
		0 min	20 min	40 min	60 min
Pt/Ba/Al-1	SO_2	0.37	0.23	0.18	0.13
Pt/Ba/Al-2	$SO_2 + O_2$	0.35	0.22	0.16	0.11
Pt/Ba/Al-3	$SO_2 + H_2$	0.37	0.18	0.13	0.10
Ba/Al-2	SO_2	0.34	0.19	0.18	0.14
Ba/Al-1	$SO_2 + O_2$	0.33	0.20	0.17	0.14
Ba/Al-3	$SO_2 + H_2$	0.33	0.20	0.16	0.14

Table 1). For the Pt-containing samples, the sample that was exposed to $SO_2 + H_2$ (Pt/Ba/Al-3) contained about 49% of the total amount of sulfur that the sample had been exposed to, and the corresponding value for Pt/Ba/Al-2 (treated with $SO_2 + O_2$) was 87%. The amount of SO_2 desorbed during the $SO_2 + O_2$ exposure and the TPD steps for the latter corresponds to about 13% of the total amount of sulfur. Thus, the sum of this and the stored amounts accounts for the entire amount of sulfur. In contrast to the $Pt/BaO/Al_2O_3$ samples, no sulfur was found in the sulfur analysis of Ba/Al-1 and Ba/Al-3 that had been exposed to $SO_2 + O_2$ and $SO_2 + H_2$, respectively.

3.5. NO_x storage and regeneration of $Pt/BaO/Al_2O_3$ and BaO/Al_2O_3 after sulfur treatments

The NO and NO_2 concentrations during NO_x storage and thermal regeneration cycles for the $Pt/BaO/Al_2O_3$ and BaO/Al_2O_3 samples that had been exposed to $SO_2 + H_2$ and $SO_2 + O_2$ are displayed in Figs. 8 and 9, respectively.

Table 3
Sulfur balance for SO_2 exposure to NO_x storage catalysts in three different exposure conditions

Sample	SO_2 exposure condition	Total $SO_{2,in}$ (mmol)	$SO_{2,out}$ step (mmol)	$SO_{2,out}$ ramp (mmol)	$S_{(trapped)}$ [a] (mmol)	Undetected S (mmol)
Pt/Ba/Al-3	$SO_2 + H_2$	0.343	0	0	0.168	0.175
Ba/Al-3	$SO_2 + H_2$	0.343	0.170	0	<0.001	0.174
Pt/Ba/Al-2	$SO_2 + O_2$	0.343	0.01	0.03	0.298	0.005
Ba/Al-1	$SO_2 + O_2$	0.343	0.104	0	<0.001	0.230

[a] Amounts of stored sulfur in the samples estimated by high temperature combustion using a LECO SC-432 sulfur analyzer.

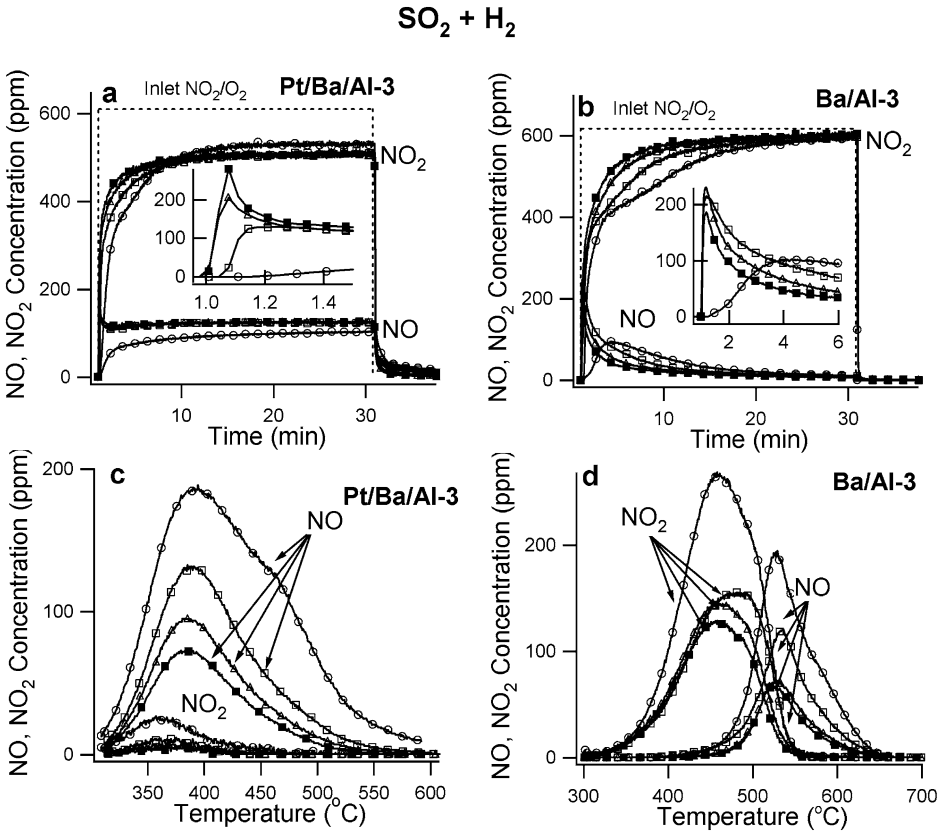

Fig. 8. NO and NO_2 concentrations as a function of time (a, b) and temperature (c, d) from one $Pt/BaO/Al_2O_3$ sample and one BaO/Al_2O_3 sample during four NO_x storage cycles using 630 ppm NO_2 and 8% O_2. Cycle 1: before exposure to sulfur, cycles 2–4: after exposure to 40 ppm SO_2 and 1.8% H_2 for 20 min prior to each NO_x storage cycle. Symbols: cycle 1 (○), cycle 2 (□), cycle 3 (Δ), and cycle 4 (■). Insets: NO concentration during the first min for cycles 1–4.

Parts a and b show the NO_x storage segments after the sulfur exposure periods (see Section 2) for $Pt/BaO/Al_2O_3$ and BaO/Al_2O_3, respectively. Parts c and d show the amount of desorbed NO and NO_2 observed during the thermal regeneration. Data from one sulfur-free NO_x storage cycle is shown for comparison. For all of the samples the inherent NO_x storage capacity is characterized by the slow rise in the NO_2 signal, as the samples are exposed to the NO_2/O_2 mixture, up to a steady-state level as the catalyst becomes saturated. Upon exposure to sulfur (both conditions), the rise in the NO_2 signal occurs more rapidly as the sulfur exposure time increases, indicating a gradual decrease in the NO_x storage capacity.

The impact of $SO_2 + H_2$ exposure on NO formation is seen clearly in Figs. 8a and 8b. For both Pt/Ba/Al-3 and Ba/Al-3 the outlet NO concentration is different after the sulfur exposure in comparison with the sulfur-free experiment. Immediately as the $NO_2 + O_2$ exposure starts after the sulfur exposure, a significant amount of NO_2 is reduced to NO. For Pt/Ba/Al-3, the amount of NO produced during the first seconds after the $NO_2 + O_2$ exposure begins increases after each sulfur exposure, whereas for the BaO/Al_2O_3 sample the opposite is true (see the insets in Figs. 8a and 8b). Furthermore, for Pt/Ba/Al-3, the NO signal reaches a stable steady-state level after all three sulfur exposure cycles, whereas for the Ba/Al-3 sample the decrease in the NO concentration continues during the entire NO_x storage period.

From Figs. 9a and 9b, it is clear that NO production during the NO_x storage cycles performed after exposure of Pt/Ba/Al-2 and Ba/Al-1 to $SO_2 + O_2$ is different from that of the sulfur-free cycle. For Pt/Ba/Al-2 the shapes of the NO response after the first sulfur exposure step and for the sulfur-free NO_x storage cycle are similar, however—almost 15 ppm higher. For the second and third cycles, only slightly more NO is produced in the beginning of the NO_x storage periods in comparison with the sulfur-free storage cycle (see the inset in Fig. 9a). The signal decreases thereafter with time (more significantly in the third cycle). The NO response from Ba/Al-1 is almost identical to the corresponding NO response from Ba/Al-3 (exposed to $SO_2 + H_2$).

As seen in Figs. 8 and 9 (c and d), the NO desorption peaks for the Pt-containing samples have maxima at around 400 °C, and almost all NO_x is completely released before the temperature reaches 600 °C for the sulfur-free cycle and 550 °C for the three sulfur-containing cycles. For the BaO/Al_2O_3 samples, the NO_2 and NO peaks have maxima at 455 and 530 °C, respectively. The NO_x release from the BaO/Al_2O_3 samples is completed at 650 °C for all four cycles.

The results from SO_2-only-treated samples are similar to those from the $SO_2 + O_2$ treatment.

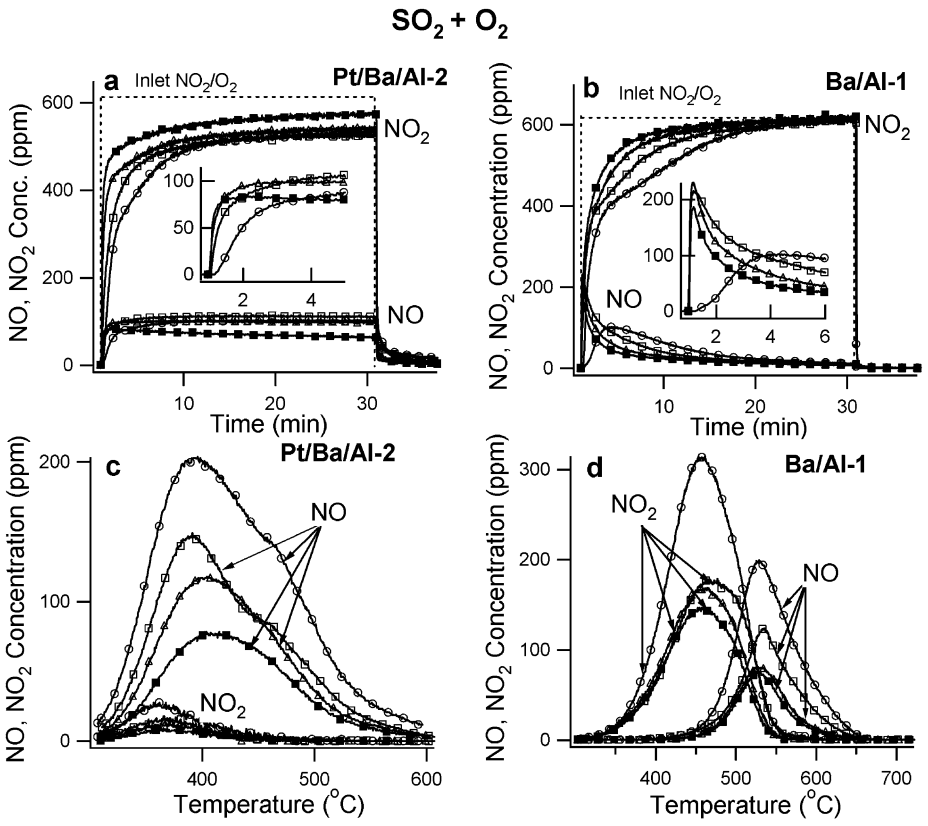

Fig. 9. NO and NO_2 concentrations as a function of time (a, b) and temperature (c, d) from one $Pt/BaO/Al_2O_3$ sample and one BaO/Al_2O_3 sample during four NO_x storage cycles using 630 ppm NO_2 and 8% O_2. Cycle 1: before exposure to sulfur, cycles 2–4: after exposure to 40 ppm SO_2 and 8% O_2 for 20 min prior to each NO_x storage cycle. Symbols: cycle 1 (○), cycle 2 (□), cycle 3 (△), and cycle 4 (■). Insets: NO concentration during the first min for cycles 1–4.

4. Discussion

4.1. NO oxidation

The aim of the NO oxidation experiments was to determine the initial catalytic activity for the Pt-containing samples before exposure to SO_2. Clearly, both the $Pt/BaO/Al_2O_3$ and the Pt/SiO_2 samples exhibit high NO oxidation activity. The NO_x outlet signal from the $Pt/BaO/Al_2O_3$ samples varies with temperature, which is not the case for the Pt/SiO_2 samples. This is probably due to NO_x accumulation on alumina and barium at low temperatures and desorption at higher temperatures. Furthermore, the Pt/SiO_2 samples show a slightly higher NO oxidation activity than the $Pt/BaO/Al_2O_3$ catalysts, although the Pt dispersion is lower for the Pt/SiO_2 samples. The increase in the activity for NO oxidation with the increase in Pt particle size (decrease in Pt dispersion) has been related to the increase in stability against Pt oxide formation for larger particles [43].

4.2. Sulfur interaction with SiO_2 and Pt/SiO_2

To investigate the interaction of sulfur with Pt, it is important to avoid or at least limit sulfur interaction with the support. Since both barium and alumina have high affinity for sulfur, silica is used in this investigation because of the inertness of silica toward SO_2 [44,45]. From Fig. 2 it is clear that no sulfur adsorption occurs on the silica sample for any of the three exposure conditions. However, this may not be the case in the presence of Pt, where SO_3 and H_2S (produced from SO_2 reaction with O_2 and H_2, respectively) may interact with SiO_2. Concerning H_2S, Wang et al. [45] found no sulfur on a SiO_2 sample exposed to H_2S at 600 °C. Although SiO_2 is considered to be the support with less affinity for sulfur in comparison with TiO_2 and Al_2O_3 [25], the adsorption of minor amounts of H_2S and/or SO_3 on SiO_2 cannot be excluded. From Fig. 2 it is clear that SiO_2 itself has no activity for SO_2 conversion under either condition (oxidation or reduction).

The consumption of SO_2 during the exposure step and the release of SO_2 during the TPD and O_2 step are two important parameters in this investigation. From Fig. 4 it is obvious that the consumption of SO_2 is much higher during $SO_2 + H_2$ exposure in comparison with $SO_2 + O_2$ exposure. Furthermore, the SO_2 conversion is stable during the entire $SO_2 + H_2$ exposure, in contrast to $SO_2 + O_2$, where the SO_2 signal increases with time. It has previously been reported that H_2S and elemental sulfur are the main products for the reaction between SO_2 and H_2 over different catalyst types [46,47]. We have confirmed the formation of H_2S (results are not shown) by using a Pt/SiO_2 catalyst in a quartz tube reactor connected to a mass spectrometer. About 100 ppm H_2S

was detected by the mass spectrometer when the sample was exposed to 370 ppm SO_2 + 2% H_2 in Ar at 300 °C (space velocity = 20 000 h^{-1}). With reference to this result and the literature data, we suggest that the consumption of SO_2 during the $SO_2 + H_2$ exposure is partially due to the formation of H_2S. Sulfur deposit on Pt is another likely product, since some SO_2 was formed during the subsequent oxygen treatment.

For the SO_2 exposure in combination with O_2, the consumption of SO_2 is lower in comparison with the case with $SO_2 + H_2$. Since SO_2 is easily oxidized in the presence of O_2, SO_3 is the most probable product during this exposure condition. The increase in the SO_2 outlet signal during the $SO_2 + O_2$ exposure indicates a decrease in SO_2 conversion, which is probably due to catalyst deactivation with time. Furthermore, the amount of SO_2 detected during the TPD is significantly higher than the corresponding amount for the $SO_2 + H_2$ exposure. The SO_2 desorption during the TPD may originate from Pt, although SiO_2 sites in the vicinity of Pt may be an additional origin for SO_2 adsorption. No SO_2 desorption was detected during the O_2 treatment, probably because no reduced sulfur species were present on the sample surface during this exposure condition ($SO_2 + O_2$).

4.3. Sulfur storage in $Pt/BaO/Al_2O_3$ and BaO/Al_2O_3

From Figs. 6 and 7 it is clear that Pt plays an important role in the storage and release of sulfur. Significantly more SO_2 is detected during the sulfur exposure steps from the BaO/Al_2O_3 samples compared with the $Pt/BaO/Al_2O_3$ catalysts. This means that the presence of Pt either gives rise to the formation of gas-phase sulfur species other than SO_2 or promotes the storage of sulfur in the washcoat. As mentioned above, SO_2 exposure in combination with H_2 or O_2 results in the formation of H_2S and SO_3, respectively. It is likely that part of the formed H_2S desorbs from the sample, whereas SO_3 most likely is trapped in the sample. This suggestion is supported by the quantitative sulfur analysis, which showed that significantly less sulfur is accumulated in the sample that was exposed to $SO_2 + H_2$ in comparison with the sample that was treated with $SO_2 + O_2$.

The stability of the sulfur compounds stored in the samples seems to be influenced by the presence of Pt. For BaO/Al_2O_3 samples weakly adsorbed SO_2 species start to desorb as soon as the SO_2 supply is switched off, which is not the case with the $Pt/BaO/Al_2O_3$ samples (see Fig. 5). No sulfur desorption is detected from the BaO/Al_2O_3 samples during the temperature ramps. It is likely that SO_2 is stored as sulfites or surface sulfates in these samples, since the formation of bulk sulfate seems to be related to the presence of Pt [48]. No sulfur was found in the samples when they were analyzed a few months after the exposure experiments, although the sulfur deactivation of the samples was obvious when the NO_x storage cycles were conducted. This implies that only weakly adsorbed sulfur species were formed in these samples. Thus, these species are expected to be replaced by carbonates (and/or hydroxyls) as the samples are kept in air.

For $Pt/BaO/Al_2O_3$ samples SO_2 desorption is only observed during the third temperature ramp (performed after the third NO_x storage cycle) and only from the sample that was treated with $SO_2 + O_2$ (see Fig. 7). It is likely that Pt lowers the sulfate decomposition temperature. However, barium sulfate may remain stable even at the end of the temperature ramps (600 °C). Thus, the desorbed SO_2 from the $Pt/BaO/Al_2O_3$ sample may originate from the decomposition of aluminum sulfate, which decomposes at temperatures $\geqslant$500 °C [35].

Sulfur storage on BaO/Al_2O_3 seems to be influenced by the exposure conditions, where in the presence of O_2 significantly less SO_2 is detected during the exposure cycles in comparison with $SO_2 + H_2$ exposure. The presence of O_2 may promote the storage of sulfur on storage sites by providing the surface with oxygen to facilitate the formation of sulfites or surface sulfates. Summers [49] found that the adsorption of SO_2 on alumina at 540 °C increased linearly with increasing oxygen concentration and suggested that impurities in the alumina (particularly Fe) may catalyze the reaction of SO_2 with oxygen, which leads to the formation of aluminum sulfite. The accumulation of sulfur on alumina in both $Pt/BaO/Al_2O_3$ and BaO/Al_2O_3 samples has previously been observed [25,35,50,51].

4.4. NO_x storage in $Pt/BaO/Al_2O_3$ and BaO/Al_2O_3 before and after sulfur treatments

The results from the sulfur-free NO_x storage cycles (shown in addition to the cycles after sulfur exposures in Figs. 8–9) indicate that samples with the same composition exhibit similar NO_x storage behaviors. However, there are significant differences between the results from the two sample types. These differences are seen in the NO and NO_2 responses (see Fig. 5). From the slope of the NO_x signals it seems that the presence of Pt slightly accelerates the NO_x storage process during the first minutes of the lean period. This is seen from the slower increase of the NO_x signal for the Pt-containing sample in comparison with the corresponding NO_x signal for the BaO/Al_2O_3 sample. The role of Pt in this respect may be connected with providing the adjacent barium sites with NO_2. The importance of NO_2 spillover between Pt and barium sites in the NO_x storage mechanism is discussed by Olsson et al. [14] in relation to mean field kinetic modeling of NO_x storage over $Pt/BaO/Al_2O_3$ catalysts. The presence of Pt in the catalyst may affect the NO_x uptake in the beginning of the storage cycles, even when NO_x is in the form of NO_2. This is indicated in data shown by Prinetto et al. [15], with a more extended period of complete uptake of NO_2, when Pt is present in the catalyst.

A comparison of the NO_x storage capacity between $Pt/BaO/Al_2O_3$ and BaO/Al_2O_3 shows that the two catalyst types have roughly the same NO_x storage capacity before the sulfur exposure (see Table 2). The sulfur-free NO_x stor-

age experiments show that the NO_x concentration for all $Pt/BaO/Al_2O_3$ samples reaches the inlet concentration after about 18 min. For the BaO/Al_2O_3 sample, the NO_x concentration is below the inlet concentration during the entire exposure time, indicating that the storage process is still proceeding (illustrated in Fig. 5). From these results, we suggest that new NO_x storage sites are slowly created in the case of the BaO/Al_2O_3 samples. This may be due to $BaCO_3$ transformation to BaO, which is suggested to be an initial step for NO_x storage [52]. For the Pt-containing samples this transformation seems to be terminated before the NO_x storage cycles have begun (probably during the calcination and/or the Pt dispersion measurements).

Below we discuss possible pathways for sulfur deterioration of the NO_x storage capacity of $Pt/BaO/Al_2O_3$ and BaO/Al_2O_3 samples:

$Pt/BaO/Al_2O_3$: The SO_2 exposure in combination with H_2 may give rise to the formation of reduced sulfur-containing species that accumulate on Pt sites and are stored on barium sites in the vicinity of Pt particles. These reduced sulfur species are then oxidized by NO_2 when the NO_2/O_2 exposure is initiated, resulting in the formation of SO_2 and SO_3, which may be trapped in the sample as surface and bulk sulfates. This oxidation process results in enhancement of NO formation during NO_x exposure, in addition to the NO, which are related to the NO_x storage process (release of one NO for adsorption of three NO_2 molecules [4,7,12,15,16,20,53]). Unlike the $SO_2 + H_2$ treatment, $SO_2 + O_2$ exposure results in the formation of SO_3 during the sulfur exposure steps. SO_3 is then trapped as bulk sulfates during the sulfur exposure step according to the following reactions:

$$SO_2 + (1/2)O_2 \rightarrow SO_3, \quad (2)$$

$$BaO + SO_3 \rightarrow BaSO_4. \quad (3)$$

This implies that NO_2 is not consumed for oxidation of surface species, as was the case with $SO_2 + H_2$ exposure. Consequently, no enhancement of NO release is observed for this exposure condition (see Fig. 9). On the other hand, the decrease in the NO_x signal with time during the third cycle in this experiment indicates that the elongated $SO_2 + O_2$ exposure may result in Pt oxide formation.

BaO/Al_2O_3: The reduction and oxidation of SO_2 by H_2 and O_2 is probably slow because of the absence of Pt in these samples. A probable pathway for sulfur accumulation and consequent deterioration of the NO_x storage sites is described by the following reactions:

$$BaO + SO_2 \rightarrow BaO\text{–}SO_2, \quad (4)$$

$$BaO\text{–}SO_2 + NO_2 \rightarrow BaSO_4 + NO. \quad (5)$$

The formation of NO in the reaction above explains the high NO concentration in the beginning of the $NO_2 + O_2$ exposure step (Figs. 8b and 9b). Interestingly, there is a decrease in NO formation with increasing sulfur exposure time, which indicates that the amount of free storage sites decreases with increased sulfur exposure time. Since no sulfur was found in the samples in the postanalysis, we suggest that only weakly adsorbed species are formed in these samples (sulfites/surface sulfates).

The decrease in the amount of available storage sites as a function of sulfur exposure time is also indicated in Figs. 8 and 9 (c and d), which display the NO and NO_2 signals recorded during the thermal treatment performed at the end of each storage cycle. For both $Pt/BaO/Al_2O_3$ and BaO/Al_2O_3 samples, the amount of desorbed NO_2 and NO observed after the NO_x storage cycles decreases with increasing sulfur exposure time.

As seen from Table 2, both samples are affected by the three sulfur exposure conditions (SO_2-only, $SO_2 + O_2$, and $SO_2 + H_2$). In the case of the $Pt/BaO/Al_2O_3$ samples, the fastest deactivation of the NO_x storage capacity is caused by the exposure to SO_2 in combination with H_2, whereas the exposure to SO_2 causes the same degree of deactivation as exposure to SO_2 in combination with O_2. Obviously, the decay in the NO_x storage capacity is not a simple function of the total amount of sulfur accumulated in the samples (see Table 3). Based on this and the similar deactivation behavior for the BaO/Al_2O_3 during all three conditions, we suggest that the presence of Pt gives rise to the formation of sulfur-containing species that may spill over to surface barium sites. The sulfur deposits on surface barium sites may result in the faster deactivation of the NO_x storage capacity, since the storage of NO_x mostly occurs on the surface layers of barium [8,54]. Recently, Wei et al. [55] highlighted the role of Pt in both the sulfation of barium and alumina and the desulfation process of the catalysts. According to the authors, Pt promotes the hydrogen spillover, which is important for the reduction of barium sulfates. That result illustrates the importance of close contact between Pt and barium for the regeneration of the NO_x storage capacity. Accordingly, as Pt particles facilitate the regeneration of the NO_x storage capacity, it is not unlikely that they play an important role in the poisoning of the NO_x storage sites.

In a previous work by Amberntsson et al. [32] the influence of SO_2 on the NO_x storage performance was studied with the use of lean (NO, O_2 and C_3H_6) and rich (NO and C_3H_6) cycles. SO_2 was added to the feed during either the lean or the rich phase. It was shown that the NO_x storage capacity declined faster upon rich SO_2 exposure in comparison with lean SO_2 exposure. The difference between lean and rich SO_2 exposure is more pronounced in the work of Amberntsson et al. [32] compared with the present study. This is probably due to differences in the NO_x regeneration process. In the present work Pt is not so important for the NO_x reduction process, since the NO_x storage sites are regenerated by heat treatment, giving thermal desorption of NO_x, and not by switching to rich conditions.

5. Conclusions

In this investigation we have exposed Pt/SiO_2, $Pt/BaO/Al_2O_3$, and BaO/Al_2O_3 samples to SO_2, $SO_2 + O_2$, and $SO_2 + H_2$ at 300 °C to study the effect of SO_2 exposure conditions on sulfur accumulation on Pt (in Pt/SiO_2 samples) and the NO_x storage performance of $Pt/BaO/Al_2O_3$ and BaO/Al_2O_3 samples. We found that the SO_2 outlet concentration over Pt/SiO_2 increased with time upon exposure to $SO_2 + O_2$ and that significant amounts of SO_2 desorb from these samples during the temperature ramps performed after the sulfur exposure steps. In contrast, upon exposure to $SO_2 + H_2$, no deactivation of Pt was observed, and only minor amounts of SO_2 desorb during the temperature ramp. However, exposure to oxygen at 700 °C resulted in SO_2 desorption, which was not the case with the SO_2 and $SO_2 + O_2$ exposures. We can therefore conclude that the exposure to SO_2 in combination with H_2 gives rise to the formation of sulfur-containing species on the samples, probably on Pt.

Both SO_2 exposures with O_2 and H_2 caused deactivation of the NO_x storage capacity of the $Pt/BaO/Al_2O_3$ and BaO/Al_2O_3 samples. However, for the Pt-containing samples the deactivation proceeded faster upon exposure to SO_2 in combination with H_2 than for the other two exposure conditions, although less sulfur was accumulated in the sample. This suggests that the sulfur-containing species that are formed during the reaction between SO_2 and H_2 interact with surface barium sites, which are important for the NO_x storage process. Moreover, we found that the presence of Pt enhances the adsorption of SO_2 under all exposure conditions. In the absence of Pt more SO_2 is adsorbed in the presence of O_2, in comparison with SO_2-only and $SO_2 + H_2$ exposures. However, there is no correlation between the total amount of adsorbed sulfur in the samples and the deactivation rate of the NO_x storage capacity. This is most probably due to the adsorption of sulfur on sites that are not necessarily important for the NO_x storage process.

Acknowledgments

This work was performed at the Competence Centre for Catalysis, which is financially supported by the Swedish National Energy Agency and the member companies: AB Volvo, Johnson Matthey-CSD, Saab Automobile Powertrain AB, Perstorp AB, AVL-MTC AB, Albemarle Catalysts, and the Swedish Space Corporation.

References

[1] R.M. Heck, R.J. Farrauto, Appl. Catal. A: Gen. 221 (2001) 443.
[2] S. Matsumoto, CATECH 4 (2000) 102.
[3] W. Bögner, M. Krämer, B. Krutzsch, S. Pischinger, D. Voigtlander, G. Wenninger, F. Wirbeleit, M.S. Brogan, R.J. Brisley, D.E. Webster, Appl. Catal. B: Environ. 7 (1995) 153.
[4] N.W. Cant, M.J. Patterson, Catal. Today 73 (2002) 271.
[5] J. Dawody, M. Skoglundh, S. Wall, E. Fridell, J. Molec. Catal. A: Chem. 225 (2005).
[6] W.S. Epling, G.C. Campbell, J.E. Parks, Catal. Lett. 90 (2003) 45.
[7] E. Fridell, H. Persson, B. Westerberg, L. Olsson, M. Skoglundh, Catal. Lett. 66 (2000) 71.
[8] D. James, E. Fourre, M. Ishii, M. Bowker, Appl. Catal. B: Environ. 45 (2003) 147.
[9] L. Lietti, P. Forzatti, I. Nova, E. Tronconi, J. Catal. 204 (2001) 175.
[10] H. Mahzoul, J.F. Brilhac, P. Gilot, Appl. Catal. B: Environ. 20 (1999) 47.
[11] I. Nova, L. Castoldi, L. Lietti, E. Tronconi, P. Forzatti, Catal. Today 75 (2002) 431.
[12] I. Nova, L. Castoldi, L. Lietti, E. Tronconi, P. Forzatti, F. Prinetto, G. Ghiotti, J. Catal. 222 (2004) 377.
[13] L. Olsson, E. Fridell, M. Skoglundh, B. Andersson, Catal. Today 73 (2002) 263.
[14] L. Olsson, H. Persson, E. Fridell, M. Skoglundh, B. Andersson, J. Phys. Chem. B 105 (2001) 6895.
[15] F. Prinetto, G. Ghiotti, I. Nova, L. Castoldi, L. Lietti, E. Tronconi, P. Forzatti, Phys. Chem. Chem. Phys. 5 (2003) 4428.
[16] F. Prinetto, G. Ghiotti, I. Nova, L. Lietti, E. Tronconi, P. Forzatti, J. Phys. Chem. B 105 (2001) 12732.
[17] F. Rodrigues, L. Juste, C. Potvin, J.F. Tempère, G. Blanchard, G. Djéga-Mariadassou, Catal. Lett. 72 (2001) 59.
[18] S. Salasc, M. Skoglundh, E. Fridell, Appl. Catal. B: Environ. 36 (2002) 145.
[19] C. Sedlmair, K. Seshan, A. Jentys, J.A. Lercher, J. Catal. 214 (2003) 308.
[20] P. Broqvist, I. Panas, E. Fridell, H. Persson, J. Phys. Chem. B 106 (2002) 137.
[21] N. Takahashi, H. Shinjoh, T. Iijima, T. Suzuki, K. Yamazaki, K. Yokota, H. Suzuki, N. Miyoshi, S.-i. Matsumoto, T. Tanizawa, Catal. Today 27 (1996) 63.
[22] N. Miyoshi, S. Matsumoto, Stud. Surf. Sci. Catal. 121 (1999) 245.
[23] A. Amberntsson, B. Westerberg, P. Engström, E. Fridell, M. Skoglundh, Stud. Surf. Sci. Catal. 126 (1999) 317.
[24] P. Engström, A. Amberntsson, M. Skoglundh, E. Fridell, G. Smedler, Appl. Catal. B: Environ. 22 (1999) L241.
[25] S.i. Matsumoto, Y. Ikeda, H. Suzuki, M. Ogai, N. Miyoshi, Appl. Catal. B: Environ. 25 (2000) 115.
[26] H. Mahzoul, P. Gilot, J.-F. Brilhac, B.R. Stanmore, Top. Catal. 16/17 (2001) 293.
[27] B.-H. Jang, T.-H. Yeon, H.-S. Han, Y.-K. Park, J.-E. Yie, Catal. Lett. 77 (2001) 21.
[28] A. Amberntsson, E. Fridell, M. Skoglundh, Appl. Catal. B: Environ. 46 (2003) 429.
[29] J.-R. Chang, S.-L. Chang, T.-B. Lin, J. Catal. 169 (1997) 338.
[30] E. Fridell, H. Persson, L. Olsson, B. Westerberg, A. Amberntsson, M. Skoglundh, Top. Catal. 16/17 (2001) 133.
[31] A. Amberntsson, M. Skoglundh, M. Jonsson, E. Fridell, Catal. Today 73 (2002) 279.
[32] A. Amberntsson, M. Skoglundh, S. Ljungström, E. Fridell, J. Catal. 217 (2003) 253.
[33] J.P. Breen, M. Marella, C. Pistarino, J.R.H. Ross, Catal. Lett. 80 (2002) 123.
[34] C. Courson, A. Khalfi, H. Mahzoul, S. Hodjati, N. Moral, A. Kiennemann, P. Gilot, Catal. Commun. 3 (2002) 471.
[35] H. Mahzoul, L. Limousy, J.F. Brilhac, P. Gilot, J. Appl. Pyrol. 56 (2000) 179.
[36] S. Erkfeldt, M. Skoglundh, M. Larsson, Stud. Surf. Sci. Catal. 126 (1999) 211.
[37] S. Poulston, R.R. Rajaram, Catal. Today 81 (2003) 603.
[38] K. Yamazaki, T. Suzuki, N. Takahashi, K. Yokota, M. Sugiura, Appl. Catal. B: Environ. 30 (2001) 459.
[39] P.T. Fanson, M.R. Horton, W.N. Delgass, J. Lauterbach, Appl. Catal. B: Environ. 46 (2003) 393.
[40] M. Skoglundh, H. Johansson, L. Löwendahl, K. Jansson, L. Dahl, B. Hirschauer, Appl. Catal. B: Environ. 7 (1996) 299.

[41] M.H. Kim, J.R. Ebner, R.M. Friedman, M.A. Vannice, J. Catal. 204 (2001) 348.
[42] P. Lööf, B. Kasemo, K.-E. Keck, J. Catal. 118 (1989) 339.
[43] L. Olsson, E. Fridell, J. Catal. 210 (2002) 340.
[44] E. Xue, K. Seshan, J.R.H. Ross, Appl. Catal. B: Environ. 11 (1996) 65.
[45] T. Wang, A. Vazquez, A. Kato, L.D. Schmidt, J. Catal. 78 (1982) 306.
[46] D.L. Murdock, G.A. Atwood, Ind. Eng. Chem. Res. 13 (1974) 254.
[47] K.-T. Li, Y.-C. Hung, Appl. Catal. B: Environ. 40 (2003) 13.
[48] Z. Liu, J.A. Anderson, J. Catal. 228 (2004) 243.
[49] J.C. Summers, Environ. Sci. Technol. 13 (1979) 321.
[50] L. Limousy, H. Mahzoul, J.F. Brilhac, P. Gilot, F. Garin, G. Maire, Appl. Catal. B: Environ. 42 (2003) 237.
[51] D. Uy, K.A. Wiegand, A.E. O'Neill, M.A. Dearth, W.H. Weber, J. Phys. Chem. B 106 (2002) 387.
[52] P. Broqvist, I. Panas, H. Grönbeck, J. Phys. Chem. B (2005), accepted submitted for publication.
[53] P. Broqvist, H. Grönbeck, I. Panas, Surf. Sci. 554 (2004) 262.
[54] J.A. Anderson, M. Fernandez-Garcia, Chem. Eng. Res. Dev. 78A (2000) 935.
[55] X. Wei, X. Liu, M. Deeba, Appl. Catal. B: Environ., in press.